Applied Catalysis A, General 667 (2023) 119444

Contents lists available at ScienceDirect

Applied Catalysis A, General

journal homepage: www.elsevier.com/locate/apcata

Wet-impregnated niobosilicate catalysts for glycerol conversion into solketal

Hussein Hussein [a], Carmela Aprile [b,*], Michel Devillers [a,*]

[a] Institute of Condensed Matter and Nanosciences, Université catholique de Louvain, Place Louis Pasteur 1, L4.01.03, 1348 Louvain-La-Neuve, Belgium
[b] Unit of Nanomaterials Chemistry, Department of Chemistry, NISM, University of Namur, Rue de Bruxelles, 61, 5000 Namur, Belgium

ARTICLE INFO

Keywords:
Mesoporous niobosilicates
Silica nanoparticles
Silica nanotubes
Glycerol acetalization
Solketal

ABSTRACT

Novel mesoporous niobosilicate materials with a homogeneous dispersion of niobium species were synthesized via impregnation of $(NH_4)_3[Nb(O_2)_2(edtaO_2)]\cdot H_2O\cdot H_2O_2$ on different hydrophilic surfaces of porous siliceous supports: extra small silica nanoparticles (XS-SiO_2) and silica nanotubes (NTs-SiO_2) bearing three different Si/Nb molar ratios of 74, 37 and 18. The Nb-silica catalysts obtained were calcined at 600 °C and then fully characterized by different physico-chemical techniques. The niobium precursor was found to be successfully loaded on the two silica support surfaces without noticeable modification of the silicate structural integrity. The Nb-containing catalysts were applied as active and selective heterogeneous catalysts for acid-catalyzed condensation of glycerol with acetone yielding solketal (2,2-dimethyl-1,3-dioxolane-4-methanol). The catalytic performance of these materials is ascribed to the enhanced accessibility of their active sites given by their morphology and to the suitable combination of acid sites. Moreover, no leaching of active sites was evidenced and the catalyst reusability studies indicated that the Nb-XS-74 and Nb-NTs-74 catalysts were successfully recyclable and highly stable in the acetalization of glycerol. The robustness and stability of the mesoporous Nb-silicate materials were also supported via characterization of the spent catalysts after the fifth recycling.

1. Introduction

In the context of green chemistry, the design of highly active and selective heterogeneous catalysts is one of the most compelling objectives of materials scientists. Heterogeneous solid catalysts that can generate sustainable fuels selectively and efficiently from renewable resources have recently received a considerable attention. Moreover, if the preparation of highly performing catalysts can be achieved through easy, time-saving and low energy consumption process, the overall sustainability of the process will increase drastically.

Nowadays, scientific investigation has gathered momentum in the field of conversion of glycerol into useful compounds especially after the massive reliance on biodiesel as a sustainable form of energy. Several approaches to employ the surplus of glycerol in different reactions have been already reported. These processes include hydrogenolysis [1], esterification [2], polymerization [3], oxidation [4] and dehydration [5]. Among the various glycerol derivatives, the synthesis of solketal via glycerol acetalization with acetone has attracted worldwide reception since solketal is largely used as a fuel additive, solvent, plasticizer and in the pharmaceutical industry as a suspension agent [6]. Additionally, solketal improves the properties of biofuel in terms of octane boosting [7].

Traditionally, acetalization of glycerol was carried out over several homogeneous acid catalysts such as p-toluene sulphonic acid, sulfuric acid, Brønsted acid ionic liquids, methane sulfonic acid and $FeCl_3.6H_2O$ [8,9]. However, most of the reported catalysts present environmental and technical limitations such as corrosion of the reactor, difficult catalyst separation, lower conversion, and high catalyst recovery cost. Heterogeneous solids as zeolites (zeolite beta) [10], resins (Amberlyst-15) [11], layered α-zirconium phosphate (ZrP-200) [12], clay minerals (montmorillonite) [13] and mesoporous silica (hafnium and zirconium modified TUD-1) [14], have been studied extensively for glycerol acetalization as promising alternatives to homogeneous catalysts due to their advantages such as their easy separation from the reaction mixture, thermal stability and high reusability. Recently, Shen et al. [15] reported excellent catalytic performance in the acetalization of glycerol with acetone under solvent free conditions using highly ordered WO_x/mesoporous SnO_2 catalyst with different WO_x loading (5–20 %wt). Also, Aguado-Deblas [16] and his group reported a sustainable, green and fast microwave assisted solketal synthesis over sulfonic

* Corresponding authors.
E-mail addresses: carmela.aprile@unamur.be (C. Aprile), michel.devillers@uclouvain.be (M. Devillers).

https://doi.org/10.1016/j.apcata.2023.119444
Received 14 July 2023; Received in revised form 6 October 2023; Accepted 8 October 2023
Available online 12 October 2023

silica-based catalysts which showed excellent performance in terms of activity, selectivity and stability with no leaching of sulfonic groups after several cycles. In addition, Jiang et al. [17] produced solketal using microporous sulfate metal organic framework (UiO-SO_3H-0.2) and exhibited prominent performance and stability compared with commercial solid acids.

Different challenges can be linked to the formation of acetals and ketals from glycerol. The first hurdle can be defined in terms of the limited miscibility between acetone and glycerol, which in turn, can be overcome using an auxiliary solvent to enhance the miscibility of the reactants. Different heterogeneous catalysts offered a sustainable and economical solution to this issue. It was reported that acetalization of glycerol achieved 97 % of solketal product using heteropolyacid PW_{12} catalyst [18,19] without the need of additional solvent, whereas blank reactions performed under same conditions but in absence of PW_{12} catalyst showed no glycerol conversion. Further analysis revealed that in absence of catalyst, the mixture glycerol/acetone was immiscible at 25 °C and a clear separation of two phases was observed. The results obtained in the presence of catalyst were explained by the fact that the catalyst increases the polarity of acetone resulting from the dissolution of PW_{12} and thus, favoring glycerol solubility. Same conclusion was drawn out by Chen et al. [20] where no glycerol conversion was recorded in blank tests at room temperature in absence of $Cs_{2.5}$ catalyst. In addition to solubility problems, another drawback of glycerol acetalization is the intrinsic production of water which slows down the reaction when excess water accumulates in the reaction mixture from one hand, and co-adsorbs close to the acid centers of the catalyst resulting in their partial deactivation from another hand [21]. To remove water from the catalytic sites, the use of a sufficiently hydrophobic catalyst without using any hazardous solvent was studied. More recently, da Silva et al. [22] reported the use of zeolite Beta with a Si/Al ratio of 16 as a catalyst for the acetalization of glycerol. The hydrophobic character of this zeolite due to high silicon content prevented the diffusion of the water into the pores, preserving the maximum activity of the acid sites and impairing the reverse reaction (hydrolysis of solketal). Another series of three-dimensional mesoporous silicate catalysts (Hf-TUD-1, Zr-TUD-1, Al-TUD-1, and Sn-MCM-41) were designed by Li et al. [14] and two of these catalysts (Hf-TUD-1 and Zr-TUD-1) showed excellent catalytic activities in solketal production, with about 65 % glycerol conversion obtained in both cases, at optimum reaction conditions. The main reasons for such a high activity were wide pores, large specific surface area, large pore size, amount of accessible acid sites, and most importantly a relatively hydrophobic surface of the catalysts. Based on what have preceded, it seems evident that a heterogeneous catalyst should be selected after careful tuning of structural and morphological features and should display proper acidity and hydrophilic-hydrophobic balance in order to favor optimum catalytic activity especially in acetalization of glycerol and other reactions yielding water as co-product such as condensation of aldehydes/ketones with alcohols [12,23–25], olefin epoxidation in the presence of H_2O_2 [26] in addition to a wide range of esterification and transesterification reactions [27,28]. The higher activity and selectivity of catalysts employed in these chemical reactions is often claimed to be related to a higher surface hydrophobicity, since water will be repelled away from the active sites due to its weak adsorption and as a result, the catalysts stability will be maintained throughout the reaction.

Among the different types of heterogeneous catalysts, mesoporous ordered silicas represented, among others, by: MCM-41 and SBA-15 (both hexagonally arranged) or MCF are among the most commonly used supports for catalytic purposes due to their regular array of pores, high specific surface area, narrow pore size distribution, large pore volume, high content surface silanol groups and high thermal and chemical stability [29,30]. Besides, a different class of silica supports is represented by the mesoporous silica nanotubes, which are of special interest because of their hydrophilic nature, easy colloidal suspension, accessibility for both inner and outer walls [31] as well as good resistance to acid and bases along with stability at high temperatures in inert or reducing atmospheres. Despite these promising features of both supports, most of possible catalytic applications of unmodified silica-based solids are hindered by the lack of acidity. However, the acid properties of the silica-based materials in terms of nature and strength of the acid sites can be finely tuned via the isomorphic substitution of silicon with a different atom (e.g. Al, Ga, Sn, Ti, Hf, etc) as single site [32–34].

Niobium-based catalysts have received special attention because of their catalytic activity in several important chemical processes, considering that they exhibit properties not revealed in catalysts containing neighboring transition metals such as V, Zr or Mo. Some of these properties, such as stability and strong metal support interaction are of utmost importance [35]. Materials containing niobium have a broad relevance in heterogeneous catalysis in line, for instance, with the promoter effect of Nb in oxidation reactions [36], and as acid catalysts for the conversion of glycerol into diglycerol, ethers and ketones [37]. The introduction of niobium in the silicate structure can therefore be a strategy to enhance the acidity of materials to be further used as efficient catalysts in various reactions. The incorporation of niobium into MCM-41 framework materials was reported by the groups of Ziolek and Ying for the first time [38]. They synthesized Nb-MCM-41 with good structural ordering and proved that all niobium present in the solid was incorporated into the silica framework. Vetrivel and Pandurangan [39] showed that the Nb-MCM-41 obtained by post-synthesis niobium incorporation was active in the vapor phase oxidation of m-toluidine into m-aminobenzoic acid. To the best of the present authors knowledge, no works have been devoted to the incorporation of niobium species on silica nanotubes supports. However, recent studies were reported dealing with the incorporation of niobium species in mesoporous cellular foam (MCF) [40].

In the context of glycerol acetalization, we recently prepared mesoporous gallosilicate catalysts [41] by the impregnation of two non-conventional Ga(III) precursors of different polarities, the neutral gallium(III) lactate monohydrate $Ga(C_3H_5O_3)_3{\cdot}H_2O$ and the ammonium salt of an anionic gallium(III) citrate complex $(NH_4)_5[Ga(C_6H_4O_7)_2].2H_2O$, on a preformed porous silica nanoparticles. The catalysts showed high activity and selectivity in the conversion of glycerol to solketal due to a fully accessible and highly dispersed surface gallium species simulating a single-site. The enhanced catalytic activity was explained in terms of acidity and the hydrophilicity of the gallosilicate materials. In this regard, Rodrigues and his group reported the synthesis of niobium-aluminum-based mixed oxide prepared by sol-gel process as highly active catalysts in the acetalization reaction [42]. In addition, Ferreira et al. [6] prepared a series of faujasite zeolite-supported niobium-based catalysts (with Nb_2O_5 amounts of 5 and 15 wt%) by impregnation of NaY, HY and HUSY zeolites using niobium(V) ammonium oxalate complex with HUSY catalyst showing the best catalytic performance (60 % glycerol conversion and 98 % selectivity to solketal at 70 °C). Recently, Kao et al. [43] synthesized SiO_2-supported niobium oxides which showed good catalytic activity in the conversion of glycerol to solketal. The conversion of glycerol was improved upon the increase of Nb loading from 5 % to 20 %wt, with Si15wt%Nb having the highest conversion (45.6 %) and yield. The high activity of Si15 %Nb was explained by the large number of acid sites being mostly Brønsted sites of strong strength, as revealed by different characterizations. Stawicka et al. [44] studied the synthesis of NbMCF materials containing exclusively Lewis acid sites and reported a glycerol conversion of 48 % under the selected optimum conditions. Also, Calvino-Casilda et al. [45] investigated the acetalization reaction over modified mesoporous cellular foams (MP-NbMCF). The catalytic materials showed the best selectivity of 99 % towards solketal even at room temperature and equimolar reactants.

The Nb precursor selected in this work is a home-made ionic water-soluble and stoichiometrically well-defined peroxo-carboxylate compound of Nb(V), $(NH_4)_3[Nb(O_2)_2(edtaO_2)]{\cdot}H_2O{\cdot}H_2O_2$ [45]. For the first

time, this niobium precursor was impregnated on two different porous silica supports, extra small (< 100 nm) porous silica nanoparticles (XS-SiO_2) and 1D- tubular silica nanotubes (NTs-SiO_2) followed by argon/air calcination at 600 °C. The physicochemical properties of the investigated niobium impregnated catalysts were characterized by powder X-ray diffraction, N_2 adsorption-desorption measurements, TEM, ICP-OES elemental analysis, FTIR, XPS, diffuse reflectance UV–Vis spectroscopy, TPD of ammonia and TGA analysis. The catalytic activity of all the niobosilicate catalysts was evaluated in the acetalization of acetone with glycerol to yield solketal under heterogeneous acid-catalyzed conditions. The catalytic results were correlated with the physico-chemical properties of the catalysts. The influence of experimental variables such as reaction time, catalyst amount, reaction temperature and acetone/glycerol molar ratio was investigated. Furthermore, the best catalysts did not suffer from leaching and were efficiently reused in successive catalytic cycles. These mesostructured materials with large and uniform pores, high surface area, and relatively suitable combination of acid sites represent an attractive alternative to the hazardous homogeneous acids with particular interest for the glycerol acetalization reaction.

2. Experimental

2.1. Synthesis of $(NH_4)_3[Nb(O_2)_4]$

The homoleptic ammonium tetraperoxoniobate complex, $(NH_4)_3[Nb(O_2)_4]$, was synthesized following a reported procedure [46]. A slurry of 3 g of niobic acid $Nb_2O_5{\cdot}nH_2O$ (supplied by CBMM) in distilled water (25 mL) was treated with a 35 wt% solution of H_2O_2 (25 mL) and ammonia (15 mL, 25 wt% solution). The cloudy solution was agitated for 5 h. When the solid is totally dissolved, addition of acetone (100 mL) yielded a white precipitate, which was filtered off, washed with acetone and air-dried. Yield: 62 %.

2.2. Synthesis of $(NH_4)_3[Nb(O_2)_2(edtaO_2)]{\cdot}H_2O{\cdot}H_2O_2$

This niobium precursor was synthesized as reported previously [47]. $(NH_4)_3[Nb(O_2)_4]$ (0.501 g, 1.82 mmol) was dissolved in 40 mL of distilled water and 5 mL of a 35 wt% H_2O_2 solution. (0.531 g, 1.82 mmol) of ethylenediaminetetraacetic acid H_4edta (Fluka) was added gradually, reaching pH = 5–5.5. The pale yellow solution was then gently heated for 10 min (T = 60 °C) and the solvent was evaporated to a final volume of 20 mL under reduced pressure. The addition of ethanol (100 mL) yielded a white solid that was filtered off, washed with ethanol, and air-dried. Yield: 70 %.

2.3. Synthesis of XS-SiO_2 and NTs-SiO_2 supports

The general protocol for the synthesis of XS-SiO_2 is inspired by a previously reported method [48]. 1.38 g of cetyltrimethylammonium bromide CTAB surfactant (TCI) was dissolved in propylene bottle in milli-Q water (628.98 g) under 800 rpm stirring at room temperature. A concentrated aqueous solution of ammonia (2 g) was added slowly to the mixture. After 30 min, tetraethyl orthosilicate TEOS (6 g) was added drop wise to the basic micellar solution under same conditions. The white solid was filtered and washed three times by milli-Q water and ethanol. The product was then dried overnight in an oven at 65 °C. Finally, the resulting solid was calcined in air to remove the organic template (5 h at 550 °C, heating rate of 3 °C min^{-1}).

Silica nanotubes (NTs-SiO_2) were prepared by a sol-gel method as previously described [49]. 1 g of Pluronic F127 $EO_{106}PO_{70}EO_{106}$ (TCI) was transferred in a covered polypropylene container and dissolved in 2 mol L^{-1} HCl (60 mL) at 11 °C under stirring at 250 rpm for 1 h. Then, a solution of TEOS (0.013 mol, 2.8 g) and toluene (3 mL) was added dropwise at 11 °C. The reaction mixture was stirred at 250 rpm for 24 h at 11 °C. Then, it was treated hydrothermally for 24 h at 100 °C. The as-synthesized material (gel) was filtered, washed with milli-Q water (600 mL) and dried overnight at 65 °C in an oven. The resulting white powder was finally calcined at 550 °C under air for 5 h (heating rate 2 °C min^{-1}).

2.4. Synthesis of Nb-XS and Nb-NTs catalysts

Different niobium-containing mesoporous silica solids have been synthesized by using wet impregnation selecting three different Si/Nb atomic ratios of 74, 37, and 18. After impregnation, materials were dried under reduced pressure at 60 °C and calcined under argon/air at 600 °C (heating rate of 2 °C min^{-1}) then in air for 5 h. The materials were denoted after calcination as Nb-XS-x and Nb-NTs-x, where x represents the atomic ratio of Si/Nb.

2.5. Niobium precursor and catalyst characterization

The niobium precursor was characterized on the basis of elemental analysis, infrared, TGA, and ^1H–^{13}C liquid NMR spectroscopy. The amount of niobium was quantified by ICP-OES elemental analysis. C-H-N elemental analyses were carried out at the University College of London. IR spectra in the 4000–400 cm^{-1} range were recorded on a FTS-135 Bio-RAD spectrometer, using KBr pellets containing ca. 1 wt% of the powder. TGA were performed in air at the heating rate of 10 °C min^{-1} using a Mettler Toledo TGA/SDTA851^e analyzer. ^1H and ^{13}C NMR spectra were measured in D_2O at 500 and 125 MHz, respectively, with a Bruker Avance 500 MHz spectrometer equipped with a broad-band inverse probe.

The silica-supported catalysts were characterized by X-ray diffraction, nitrogen physisorption, transmission electron scanning, ICP-OES elemental analysis, X-ray photoelectron spectroscopy, diffuse reflectance UV–visible spectroscopy (DR UV–vis), Fourier transform infrared spectroscopy, ammonia temperature-programmed desorption and TGA analyses.

Powder X-ray diffraction (XRD) patterns were measured on a PANalytical X′pert pro diffractometer with Cu Kα radiation (λ = 1.54178 Å).

Specific surface area and porosity of the solids were determined from the nitrogen adsorption–desorption isotherms obtained at 77 K with a volumetric adsorption analyzer Micromeritics Tristar 3000. The samples were pretreated at 150 °C for 24 h under a reduced pressure of (0.1 mbar). The Brunauer–Emmett–Teller (BET) method was used to calculate the specific surface areas in the p/p_0 = 0.05–0.30 range. The pore size distributions were calculated from the adsorption branch of the isotherm using the Barrett–Joyner–Halenda (BJH) method with the Kruk-Jaroniec-Sayari (KJS) correction.

Transmission electron microscopy (TEM) images were recorded on a Philips Tecnai 10 microscope operating at 80 kV. Samples were prepared by dispersion of a small quantity of material in absolute ethanol and deposited onto a copper grid.

Fourier transform infrared spectroscopy was used in attenuated reflectance modes using an IFS55 Equinox spectrometer Bruker equipped with a DTGS detector. The spectra were obtained by recording 100 scans in the range from 800 to 4000 cm^{-1} with a 4 cm^{-1} resolution. The spectra were analyzed using the software OPUS.

Diffuse reflectance UV–vis spectra were measured in a spectral range from 200 to 550 nm using the Cary Win UV software package and a CARY 5000 Agilent spectrometer equipped with a Praying Mantis.

The niobium loading was quantified by inductively coupled plasma optical emission spectrometry. 10 mg of each sample was dissolved in a mixture of 100 μL of aqua regia and 600 μL of aqueous HF. The obtained solutions were analyzed using an Optima 8000 ICP-OES Spectrometer.

The XPS analyses were carried out with a SSX 100/206 photoelectron spectrometer from Surface Science Instruments (USA) equipped with a monochromatized micro focused Al X-ray source (1486.6 eV) and powered at 20 mA and 10 kV. The powdery samples were fixed with double-sided tape onto small brass troughs of 6 mm diameter that were

placed on a ceramic carousel. The pressure in the analysis chamber was around 10^{-6} Pa. The angle between the surface normal and the axis of the analyzer lens was 55°. The analyzed area was approximately 1.4 mm^2 and the pass energy was set at 150 eV. In these conditions, the full width measured at half maximum (FWHM) of the Au $4f_{7/2}$ peak for a clean gold standard sample was about 1.6 eV. A flood gun set at 8 eV and a Ni grid placed 3 mm above the sample surface were used for charge stabilization. The following sequence of spectra was recorded: survey spectrum, C 1 s, O 1 s, Si 2p, Nb 3d and C 1 s again to check the stability of charge compensation with time. The Si 2p peak was chosen as the best compromise for calibration by fixing its position at 103.5 eV. The Nb 3d doublet was decomposed by fixing the distance between Nb $3d_{5/2}$ and Nb $3d_{3/2}$ to 2.78 eV and by constraining their intensity ratio to the expected theoretical value of 3:2. Data treatment was performed with the CasaXPS program (Casa Software Ltd, UK), some spectra were decomposed with the least squares fitting routine provided by the software with a Gaussian/Lorentzian (85/15) product function and after subtraction of a non-linear baseline. Molar fractions were calculated using peak areas normalized based on acquisition parameters and sensitivity factors provided by the manufacturer.

Temperature-programmed desorption of ammonia (NH_3-TPD) was carried out to evaluate the total acidity of the catalysts. Around 50 mg of sample was introduced in a quartz reactor on a Hiden Analytical Catlab-PCS apparatus. Prior to measurement, the sample was preheated in argon flow (30 mL min^{-1}) at 200 °C for 2 h. Subsequently, it was cooled down to 50 °C and then exposed to a gas mixture of 5 % NH_3 in He (10 mL min^{-1}) and Ar (20 mL min^{-1}) for 45 min. Physisorbed NH_3 was removed by purging with Ar (30 mL min^{-1}) at 50 °C for 90 min. The TPD measurement was conducted by heating the sample from 50° to 650°C with ramping rate of 5 °C min^{-1}. Desorbed NH_3 was detected by a mass spectrometer (QGA model).

Thermogravimetric analyses (TGA) were carried out under inert atmosphere (nitrogen gas flow of 90 mL min^{-1}) using a Mettler Toledo TGA/SDTA851^e analyser, with a heating rate of 10 °C min^{-1} in the range 25–900 °C. Following a previously reported procedure [50], all samples were pretreated for 72 h in a desiccator containing a saturated aqueous solution of NH_4Cl to reach the maximum level of water adsorption. The hydrophilicity of the materials was estimated from the number of water molecules adsorbed on the surface of each sample, calculated from the mass loss between 25 and 200 °C measured by TGA, using the following equation:

$$n_{H_2O} = \frac{\Delta m}{m_i} \times \frac{N_A}{S_{BET} \times M_{H_2O}}$$

where nH_2O is the number of adsorbed water molecules per nm^2 of catalyst surface; Δm is the mass loss between 25 and 200 °C (g); m_i is the initial mass of the sample at 25 °C (g); MH_2O is the molar mass of water (18.0153 g mol^{-1}); S_{BET} is the surface area calculated from the nitrogen adsorption-desorption isotherms (nm^2 g^{-1}); N_A is the Avogadro constant.

2.6. Catalytic tests

The liquid phase acetalization of glycerol was accomplished under solvent-free conditions in 10 mL round bottom flask under vigorous stirring (800 rpm) at 50 °C. In a typical catalytic test, 0.921 g of highly purified glycerol (purity 99 %, 0.01 mol), 2.32 g of acetone (0.04 mol) and 10 mg calcined of catalyst were weighed and the mixture was stirred for 6 h at the selected temperature. Then, the mixture was cooled down to room temperature and homogenized via the addition of 3 mL of absolute ethanol. Then, the catalyst was separated by centrifugation (4500 rpm, 10 min). 500 μL of the supernatant were taken from the filtrate and the solvent was evaporated under reduced pressure. Finally, 600 μL of DMSO as a deuterated solvent were added for quantitative ^{1}H NMR analysis. 2,2-dimethyl-1,3-dioxolane-4-methanol (solketal): ^{1}H NMR (400 MHz, DMSO-d_6): δ = 4.78 (1 H, t, –OH), 4.03 (1 H, m, –CH–), 3.94 (1 H, dd, $–CH_2–CH–$), 3.63 (1 H, $–CH_2–CH–$), 3.42 (1 H, m, $–CH_2–OH$), 3.35 (1 H, m, $–CH_2–OH$), 1.30 (3 H, s, $–CH_3$), 1.25 (3 H, s, $–CH_3$).

Recyclability tests were performed by centrifuging the sample obtained at the end of the catalytic test after which the solution was removed. Then, the catalyst was washed five times with absolute ethanol followed by centrifugation. Afterwards, the catalyst was calcined at 500 °C for 5 h (heating rate of 2 °C min^{-1}). The subsequent catalytic tests were carried out by repeating this procedure from the beginning (the quantities were adapted as a function of the mass of the recovered catalyst).

Leaching tests were performed at 50 °C under 800 rpm stirring by dissolving glycerol (0.01 mol) in 0.7 mL of absolute ethanol with 2 min sonication followed by addition of 25 mg of calcined catalyst and acetone (0.04 mol). The catalyst was removed from the reaction mixture after 1 h by hot filtration using a plastic syringe equipped with a 25 mm syringe filter, with a pore size of 0.2 μm, then followed by centrifugation at the same temperature. The filtrate was allowed to react for another 5 h. The reaction mixture was analyzed by ^{1}H NMR after 1 h and at the end of the filtrate test (6 h).

3. Results and discussion

3.1. Characterization of the catalysts

The water-soluble peroxo complex of niobium(V) with ethylenediaminetetraacetic acid (H_4edta) corresponding to the formula $(NH_4)_3[Nb(O_2)_2(edtaO_2)]\cdot H_2O\cdot H_2O_2$ has been prepared as reported previously by partially replacing peroxo groups of the tetraperoxoniobate anion $[Nb(O_2)_4]^{3-}$. The synthesis was carried out in the presence of an excess of hydrogen peroxide, which led to the direct formation of the bis(N-oxide) derivative of the PAC ligand. The complex was characterized via different techniques including combustion chemical analysis, IR and NMR (^{1}H, ^{13}C) spectroscopy and TGA. In addition, the Nb loading was quantified by ICP analysis. All the characterization data were in agreement with those reported previously by Bayot et al. [47] and allowed confirming the structure and purity of the complex. Then the Nb(V) precursor was impregnated onto two silica supports with different morphologies: XS-SiO_2 and NTs-SiO_2. These two catalytic supports were selected due to their well-defined structure, high specific surface area and controllable properties as morphology, narrow pore size distribution, small uniform size and good thermal stability. The synthesized peroxo Nb(V) precursor seems to be an adequate candidate because of its high solubility in water which makes it suitable for the preparation of supported-silica catalysts by wet impregnation in contrast to other commercial niobium precursors such as niobic acid, pentachloride $NbCl_5$ and some Nb alkoxides $Nb(OR)_5$ [51]. After impregnation, the solvent was evaporated and the materials were submitted to controlled thermal treatment under argon followed by air at 600 °C to ensure the complete removal of the organic ligands. The initial presence of argon should favor the formation of stable Si–O–Nb bonds and well dispersed single site-like species, while decreasing the possibility of migration and sintering with generation of less active Nb_2O_5 aggregates. The calcination temperature was determined from the TGA profile of the Nb(V) precursor (Fig. S1). After dehydration, the complex undergoes a three-step degradation into Nb_2O_5 up to a final decomposition temperature of 620 °C. A temperature screening from 550 °C to 620 °C was performed in order to find the optimum calcination temperature. It was decided to heat the Nb-based catalysts at 600 °C in order to preserve their acidic properties, since calcination above this temperature could damage the silica structure, thus causing a loss in surface area and a decrease in number and strength of acid sites especially with Nb-NTs catalysts. Besides, a calcination temperature below 600 °C might not remove fully the organic ligands from the catalysts as inferred from the TGA profile of the Nb(V) precursor (Fig. S1).

Table 1
Textural properties of the studied catalysts.

Material	BET surface area (m^2/g)	Pore size (nm)	Pore volume (cm^3/g)
XS-SiO_2	1310	2.6	2.27
Nb-XS-74	1167	2.5	1.79
Nb-XS-37	1020	2.4	1.56
Nb-XS-18	925	2.3	1.41
NTs-SiO_2	753	15.2	2.14
Nb-NTs-74	670	14.9	1.82
Nb-NTs-37	620	14.7	1.73
Nb-NTs-18	570	14.5	1.52

Two series of mesoporous Nb-silicate materials were prepared: Nb-XS samples with extra-small (XS) nanoparticles morphology and Nb-NTs with tubular morphology. Three different Si/Nb atomic ratios of 74, 37 and 18 were selected. Prior to the catalytic tests, the physico-chemical and structural features of the synthesized materials were investigated by various techniques mentioned above.

N_2 adsorption-desorption analysis was carried out to determine the specific surface area, pore volume and pore size distribution of all samples (Table 1). In both series, the Nb-loaded materials display lower specific surface areas and pore volumes than the pristine supports. This reduction in the specific surface area and pore volume at different Si/Nb ratios could be attributed to the uneven distribution of Nb-based species and the formation of small niobium oxide aggregates causing the partial obstruction of the pores. Similar decrease in surface area and pore volume was also reported upon the loading of Nb on MCF support [40]. Noticeably, at low Nb content (Nb-XS-74 and Nb-NTs-74), the catalysts exhibit higher specific surface areas and pore volumes as well as slightly larger mesopores than the corresponding solids containing a higher amount of niobium (Nb-XS-37 and −18; Nb-NTs-37 and −18). The surface area, pore volumes and pore sizes reveal the mesoporous nature of both series of niobium containing silicates. As expected, all Nb-XS catalysts displayed a type IV isotherm which is the characteristic feature of mesoporous materials. A clear hysteresis loop at higher relative pressure was clearly observed and attributed to disordered inter-particle cavities originated as consequences of the small particle size (Fig. 1**a**). The BJH pore size distribution of Nb-XS materials displayed a narrow peak centered at 2.3–2.6 nm for all catalysts along with a broad band between 15 and 50 nm due to the presence of interparticle voids (second type of porosity) (Fig. 2**a**). These finding are in agreement with

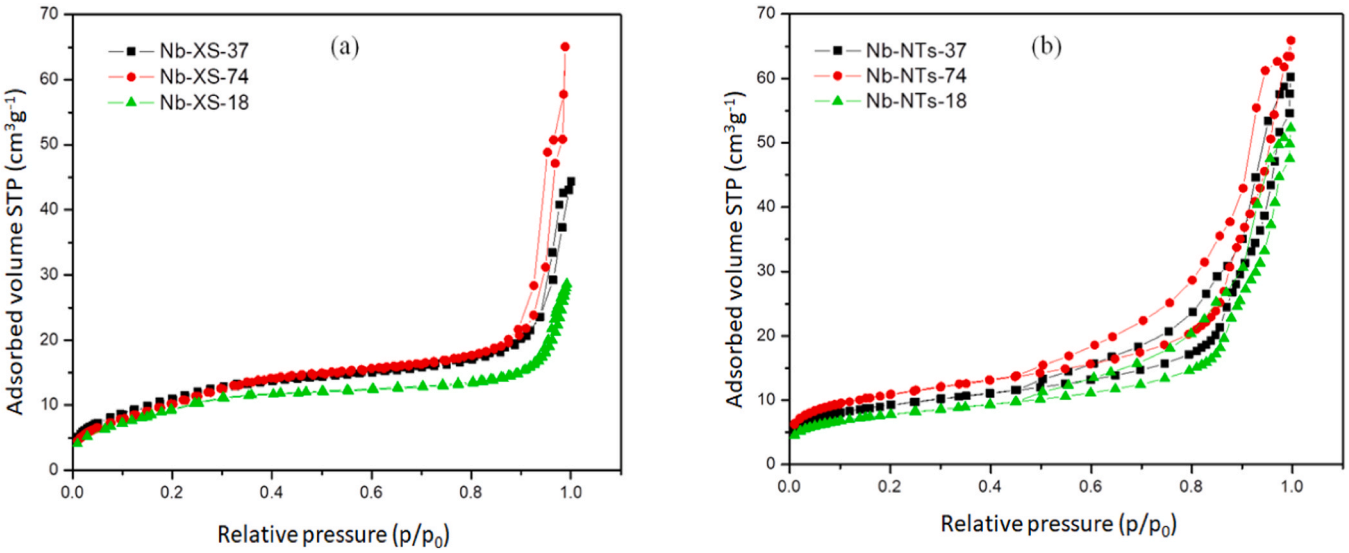

Fig. 1. Nitrogen physisorption isotherms of (a) Nb-XS and (b) Nb-NTs catalysts.

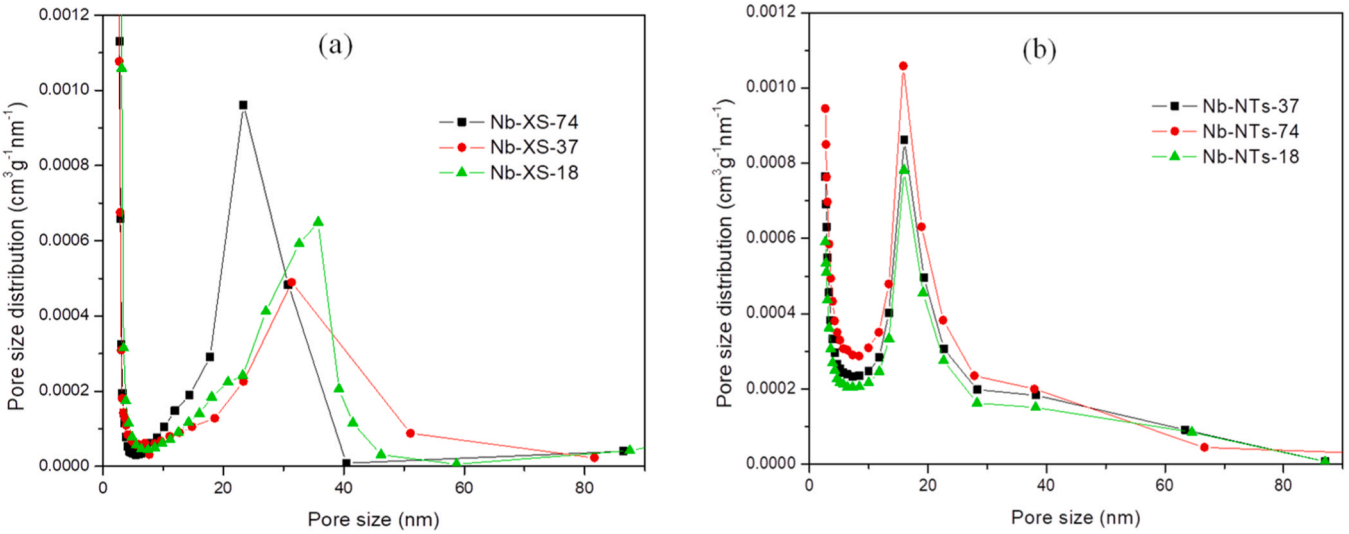

Fig. 2. Pore size distribution profiles determined by BJH method of (a) Nb-XS and (b) Nb-NTs catalysts.

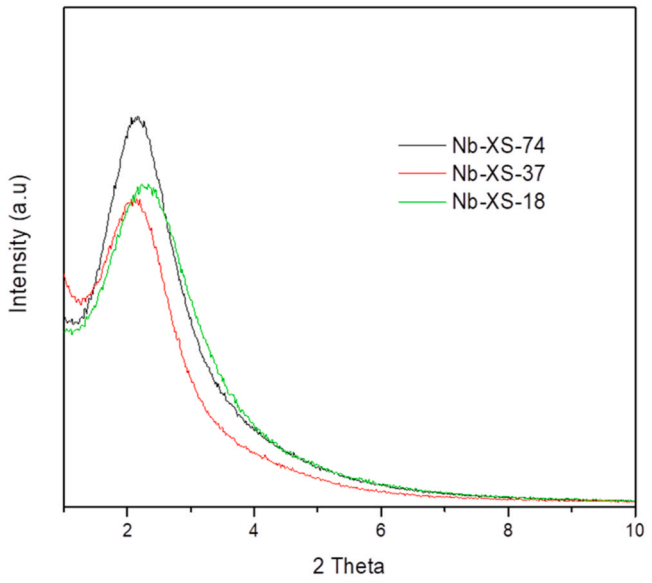

Fig. 3. PXRD pattern of Nb-XS catalysts.

our previous study concerning gallium mesoporous silicates [41]. Saini et al. [52] also reported the presence of modernite-based catalysts with mesopores in the range of 5–50 nm and many other heterogeneously distributed pores being attributed to the interparticle voids. In the case of Nb-NTs isotherms, the capillary condensation appearing at high relative pressure (around 0.9) indicated the presence of large mesopores. The adsorption-desorption loop observed in all Nb-NTs can be considered as a combination of two different contributions due to presence of tubular structures as well to disordered cavities generated by the entangled nanotubes (Fig. 1**b**). More importantly, the narrow hysteresis loop with the presence of a tail indicated that most pores were without any constrictions [49]. Due to the entangled nature of nanotubes, the pore size distribution was estimated via the Barrett-Joyner-Halenda (BJH) using the Kruk-Jaroniec-Sayari (KJS) correction [53,54]. Two distinct porosities can be clearly distinguished, the first and better defined contribution centered at around 14 nm could be attributed to the internal void of the 1D structure, while the second broader band was ascribed to the irregular inter-tubular spaces (Fig. 2**b**). These observations are in line with previous studies reported for silica-based nanotubes subjected to hydrothermal treatment [34,49,55].

Low angle powder X-ray diffraction performed on Nb-XS samples exhibit a broad and intense diffraction peak, which can be attributed to the hexagonal structure of the mesoporous material and is assigned to the d_{100} diffraction (Fig. 3). The incorporation of Nb into the structures of XS-SiO_2 and NTs-SiO_2 supports by post-synthesis method revealed a diffraction pattern closely matching the parent materials, indicating that the mesoporous structure is preserved after impregnation with the niobium species and subsequent calcination at 600 °C. The diffraction pattern of the anhydrous Nb_2O_5 observed at $2\theta = 22.4°$, 28.4°, 36.7°, 46.1°, 50.7° and 55.2° can be indexed to the orthorhombic (T) phase of niobium pentoxide [56]. More importantly, the presence of aggregates of Nb oxide or other Nb phases during the synthesis or the thermal treatment was not detected which agrees with previously reported studies [40]. All the calcined samples, even those at very high niobium content, are completely amorphous (Fig. S2). A careful analysis of the diffractogram allows excluding a possible phase separation since no defined XRD reflection attributable to crystalline Nb_2O_5 was observed. This result indicates that the Nb species are mainly inserted in an amorphous environment even if the existence of niobium oxide particles of very small size on the silica surfaces cannot be completely excluded. In addition, the high calcination temperature at 600 °C did not have a significant influence on the structural morphologies of both classes of materials.

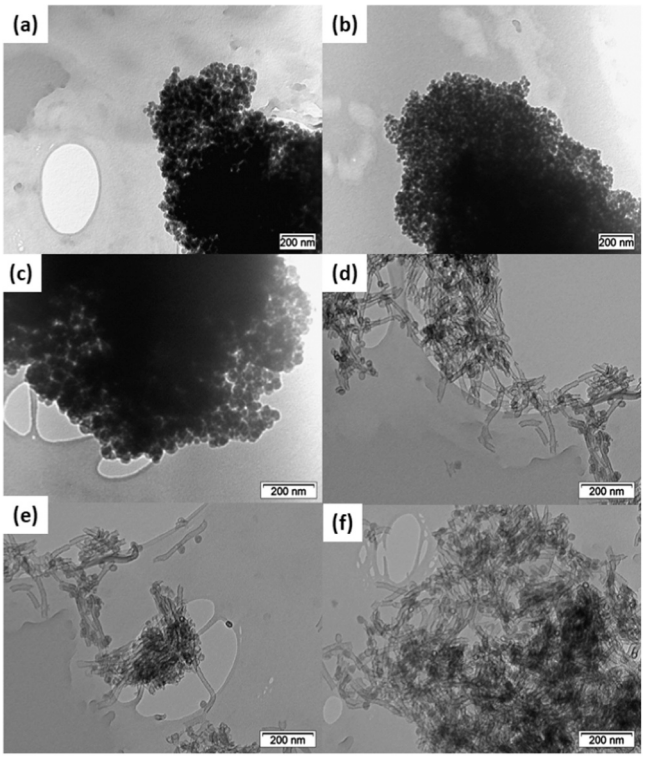

Fig. 4. TEM images of (a) Nb-XS-74, (b) Nb-XS-37, (c) Nb-XS-18, (d) Nb-NTs-74, (e) Nb-NTs-37 and (f) Nb-NTs-18.

The morphological properties of the solids were determined with the help of transmission electron microscopy (TEM). TEM demonstrated that Nb-XS catalysts (Fig. 4**a, b and c**) consisted of nanosized spherical particles typical of mesoporous SiO_2-like materials. TEM micrographs confirmed the presence of extra small mesoporous niobosilicates with well-organized hexagonal pores even at high Nb loading. Moreover, in all cases, some zones of condensation between the different particles are present. This observation is in agreement with the presence of the interparticle voids suggested by the N_2-physisorption analysis. TEM performed on Nb-NTs mesoporous solids (Fig. 4**d, e and f**), revealed mainly the presence of well-defined tubes with clearly visible walls. Small fraction of nanospheres was observed, perhaps as a result of a budding process [57] that resulted in the fragmentation of the nanotubes to nanospheres. The nanostructures exhibited an average diameter of about 20 nm with an inner porosity of ca 15 nm. After calcination, the appearance of nanostructures of reduced length was observed indicating that the thermal treatment resulted in a partial cleavage of some tubes into smaller fragments. For some nanotubes, round ends with somewhat higher diameter than the diameter along the tubes were observed, which is consistent with earlier experimental and theoretical studies of worm-like micelles [58]. From an in-depth TEM investigation, no noticeable differences emerged comparing the morphology of the three samples in both series. Therefore, raising the concentration of Nb, in the selected range, does not influence the final tubular morphology of the solids. In addition, TEM investigation allowed confirming the absence of large separate domains of niobium oxide species at the surface of the silica-based supports indicating a homogeneously dispersed Nb species into the mesoporous silica framework which is in agreement with the PXRD. Despite the fact that TEM investigation on NTs-based catalyst did not evidence the presence of small aggregates of Nb oxide species, the decrease of the specific surface area observed via N_2 physisorption can be ascribed to the presence of small particles of niobium oxide probably too small to be detected via TEM analysis.

The amount of niobium incorporated in the different solids was

Table 2
XPS data (binding energies and Nb/Si atomic ratio) of the studied catalysts.

Catalyst[a]	O 1s (eV)	Nb $3d_{5/2}$ (eV)		Surface Si/Nb[b]	Bulk Si/Nb[c]	Surface Nb/Si[b]	Bulk Nb/Si[c]
Nb-XS-74	532.8	207.1	208.9	91	80	0.010	0.012
Nb-NTs-74	532.7	207.0	208.2	95	82	0.010	0.012
Nb-XS-37	532.8	207.1	208.6	54	35	0.018	0.028
Nb-NTs-37	532.8	207.1	209.0	56	34	0.017	0.029
Nb-XS-18	532.7	207.2	208.7	29	20	0.034	0.050
Nb-NTs-18	532.7	207.1	208.9	32	21	0.031	0.047
Nb_2O_5	530.2	-	207.1	-	-	-	-

[a] Nominal ratio employed during the synthesis is Si/Nb = 74, 37 and 18.
[b] Determined by XPS.
[c] Determined by ICP-OES.

quantified by inductively coupled plasma optical emission spectrometry (ICP-OES) and the resulting Si/Nb ratios (Table 2) in all the calcined mesoporous materials were in excellent agreement with the theoretical ratios.

XPS analyses were conducted in order to investigate the surface composition and the quality of the Nb dispersion at the surface. The XPS data are summarized in Table 2. Due to some uncertainties with usual carbon referencing for the calibration of the energy scale, Si 2p peak was chosen as the best compromise for calibration by fixing its position at 103.5 eV. This assumes that the BE of the Si 2p peak is not affected by some interaction with Nb, as most of Si is present as SiO_2 with such a high Si/Nb proportion. The O1s region of anhydrous Nb_2O_5 calcined at 600 °C (taken as a reference) displayed a peak at lower BE value (530.2 eV) than those of the Nb-silicate catalysts, which showed single and almost symmetric peaks in the BE range 532.7–532.8 eV, close to the value in SiO_2 (533.0 eV) (Fig. S3). The Nb 3d XPS spectrum of Nb_2O_5 (Fig. 5 **g**) consists of a clearly narrow and well resolved doublet composed of the Nb $3d_{5/2}$ and Nb $3d_{3/2}$ contributions, decomposed with the two constraints of an energy difference of 2.78 eV and a 1.5:1 intensity ratio. In the following, only the BE of the more intense Nb $3d_{5/2}$ peak will be discussed. A single Nb $3d_{5/2}$ at 207.1 eV was obtained in Nb_2O_5 that differs from those observed in both series of synthesized materials, which showed broader and less resolved doublets, indicating that probably more than one Nb chemical state should be considered to properly decompose the spectra according to the doublet characteristic shape. Good fits were obtained with a series of two doublets (red and blue in Fig. 5). The lowest Nb $3d_{5/2}$ BE (red), close to 207 eV, is attributed to Nb_2O_5 while the other one, shifted to higher BE than 208.0 eV, can be attributed to dispersed Nb species on the supports or related to the change in the Nb coordination upon formation of Nb-O-Si linkages [59,60]. The Nb $3d_{5/2}$ binding energy of 209.5 eV was reported for NbSBA-15 containing mostly isolated sites with tetrahedral coordination [61], while for MCM-41-supported niobium oxide catalysts, the BE values were in the range of 207.5–208.0 eV [62]. Similar findings were reported for NbMCF catalysts where the high value of $3d_{5/2}$ BE (207.6 eV) confirmed the incorporation of Nb species in the mesoporous silica matrix [40]. Note that in these studies all binding energy (BE) measurements were corrected for charging effects with reference to the C 1s peak of the adventitious carbon (284.6 eV). Considering that the presence of Nb_2O_5 in all our samples was not detected previously by PXRD analysis, the Nb oxide species are assumed to be amorphous or as very small size particles. Table 2 shows the comparison between the surface Nb/Si atomic ratios determined by XPS and those corresponding to the bulk atomic ratio obtained from ICP-OES. In both series of catalysts with higher Nb loading (Si/Nb of 37 and 18), the surface Nb/Si atomic ratios are lower than the bulk ratios, which reveals no surface enrichment of Nb species.

Diffuse reflectance (DR) UV–vis spectra of the niobosilicate catalysts are shown in Fig. S4. According to the literature, the DRS UV absorption band at 220–270 nm can be assigned to the charge-transfer transition between oxygen atoms and isolated Nb(V) centers, presumably, in tetrahedral coordination or penta-coordinated, both typical of niobium located in the silica matrix [40,63–65]. In our studied Nb-silicate catalysts, the presence of a non-resolved band in the region 220–270 nm could be tentatively ascribed to the presence of a combination of various Nb species in different coordination environments at the surface. Importantly, for all the niobosilicate materials, no absorptions were detected above 400 nm, indicating that no large Nb_2O_5 domains were present on the catalyst surface [60], suggesting a homogeneous dispersion of Nb species throughout the silica framework as previously inferred from PXRD.

The FT-IR spectra of pure XS-SiO_2 and NTs-SiO_2 and the niobosilicate samples are shown in (Fig. 6**a and b**). All the samples exhibited IR bands in the region 3400–2400 cm^{-1} due to surface –OH groups and a IR band at 1630 cm^{-1} assigned to the bending mode of the water molecule [52]. In general, the typical siliceous materials exhibit IR bands in the range of 400–2000 cm^{-1}. The IR spectra of the pure silica supports exhibited a main IR band at 1080 cm^{-1} and a weaker band at 800 cm^{-1} due to antisymmetric and symmetric stretching modes of the Si–O–Si bond. In addition, a strong IR band at 458 cm^{-1} can be attributed to the rocking of the Si–O–Si bond. The IR spectra of all Nb-silicate samples showed the IR bands similar to that of the pure XS-SiO_2 and NTs-SiO_2. The band at 960 cm^{-1} is present in the pristine material (without Nb) as well as in the Nb-based catalysts in which it is visible as a shoulder because of a very high intensity of the band at 1080 cm^{-1}, revealing that it origins not only from Si–O–Metal linkage but also from Si–OH present in silica. Therefore it cannot be assigned only to Si–O–Nb species. As a result, IR spectra cannot exclusively evidence of the formation of Si-O-Nb bonds in the Nb-containing samples and the incorporation of Nb and the formation of Si-O-Nb linkage in the silica matrix were mainly evidenced by the XPS measurements as inferred previously.

The strength and amount of acid sites of all the synthesized catalysts were revealed by temperature-programmed desorption of ammonia (NH_3-TPD) (Fig. 7 **and** Table 3). The peaks at lower temperature (less than 200 °C) are due to the weak acid sites, while those at moderate temperature (centered at 250 °C) refer to the release of ammonia from medium acid sites. As clearly seen, Nb-XS-74 and Nb-NTs-74 catalysts showed a greater desorption area for ammonia, revealing their higher concentration of acid sites whereas, Nb-XS-18 and Nb-NTs-18 had the lowest acid sites population. Besides, all XS-based catalysts have higher acidic population than their NTs-based analogues with the same Si/Nb molar ratio. The quantitative results calculated from the NH_3-TPD (Table 3**)** indicate a relationship between the niobium loading and the population of acid sites. For both series of catalysts, the increase in the metal loading leads to a gradual decrease in the acid sites concentration. This may be due to the fact that as the Nb loading increases, some extra-framework niobium oxide species may form. These niobium oxide species should be in the form of very small particles or short oligomeric chains hence not visible in the XRD pattern.

The incorporation of niobium is expected to favor the formation of both Brønsted (BAS) and Lewis acid sites. The generation of BAS is mainly related to the bridged Nb-OH-Si (with surface intra-framework niobium in a tetrahedral environment), but the contribution of Nb-OH-Nb species should be also considered. In addition, the niobium oxide evidenced by XPS in all the samples may be in the form of surface NbO_4 tetrahedral sites or surface NbO_6 octahedral sites associated to Lewis acid sites.

To evaluate the hydrophilicity of the catalysts, thermogravimetric analysis (TGA) was performed. The number of adsorbed water molecules on the surface of each catalyst (nH_2O/nm^2) was calculated according to formula mentioned in the experimental section and results are listed in

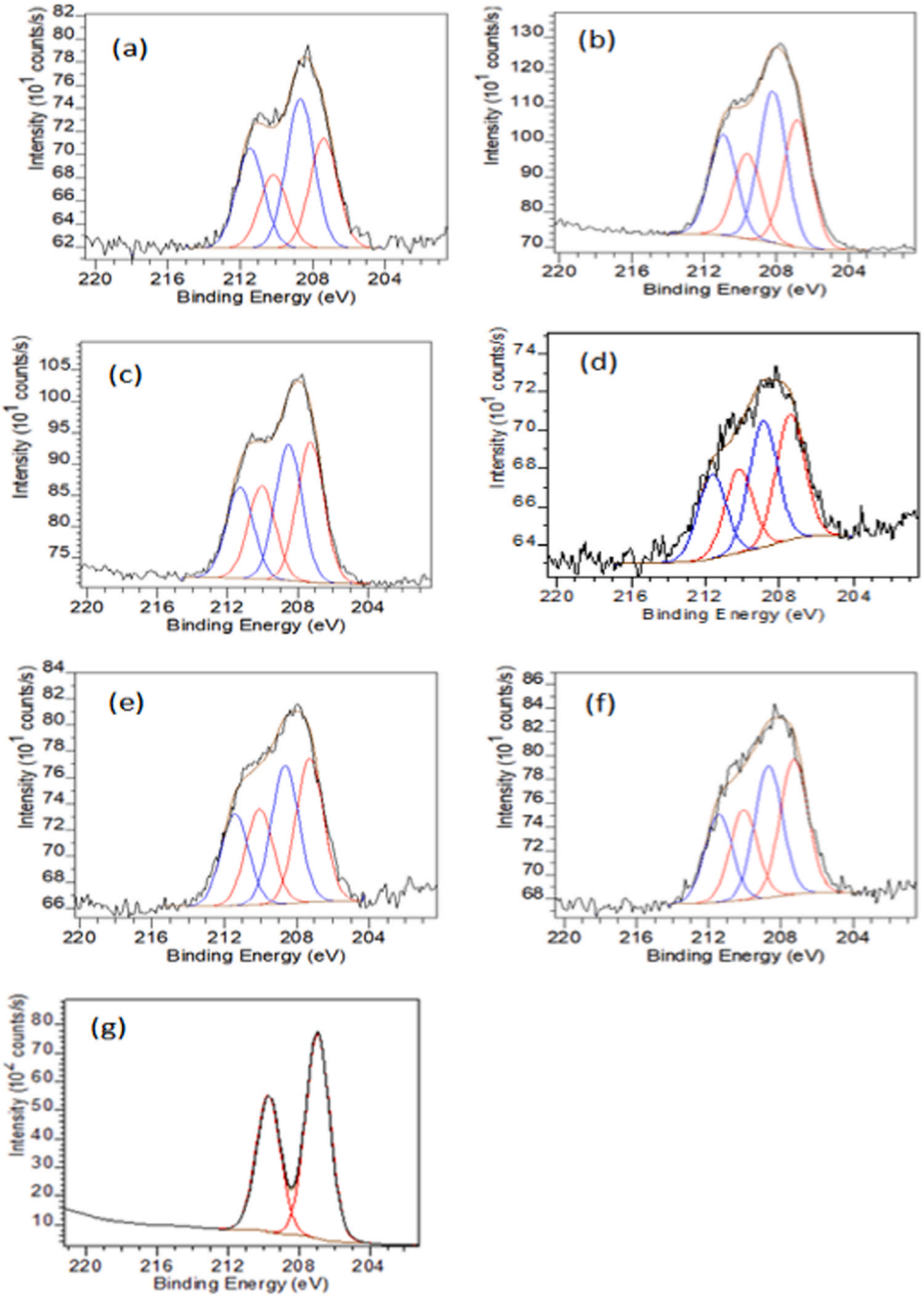

Fig. 5. XPS spectra of the Nb 3d regions of (a) Nb-XS-74, (b) Nb-NTs-74, (c) Nb-XS-37, (d) Nb-NTs-37, (e) Nb-XS-18, (f) Nb-NTs-18 and (g) Nb_2O_5.

Table S1. The data revealed that the hydrophobic character decreases in the following order: Nb-XS-74 > Nb-NTs-74 > Nb-XS-37 > Nb-NTs-37 > Nb-XS-18 > Nb-NTs-18. In line with the fact that pure XS-SiO_2 support is more hydrophobic than NTs-SiO_2, all XS-based catalysts have a relatively more hydrophobic surface than NTs ones at a given Si/Nb molar ratio. Moreover, in both series of materials, the hydrophilicity increases with the Nb loading and is the highest for the sample with the Si/Nb molar ratio of 18.

From the above characterizations, it emerged that these mesoporous niobosilicate catalysts present a favorable combination of catalytic features such as high surface area, highly accessible acid sites and insertion of well-dispersed niobium species simulating as single site in the silica framework.

3.2. *Glycerol acetalization to solketal*

Combining the results obtained from NH_3-TPD and TGA, it can be evidenced that mesoporous niobosilicates (Nb-XS-74 and Nb-NTs-74) present the highest acidic population and a relatively hydrophobic surface compared to the other studied catalysts in addition to promising textural properties which are all expected to have a positive impact on the performance of the catalysts in the conversion of glycerol to solketal. A kinetic study was performed using Nb-XS-74 and Nb-NTs-74 as catalysts for the acetalization of acetone with glycerol at 50 °C with acetone/glycerol molar ratio of 4/1 (Fig. 8). In both tested catalysts, the solketal yield tends to reach a plateau after 15 h when 10 mg of catalysts were used. To confirm this, two additional tests were performed with extra 10 mg of fresh catalysts being added after 24 h of the reaction at 50 °C.

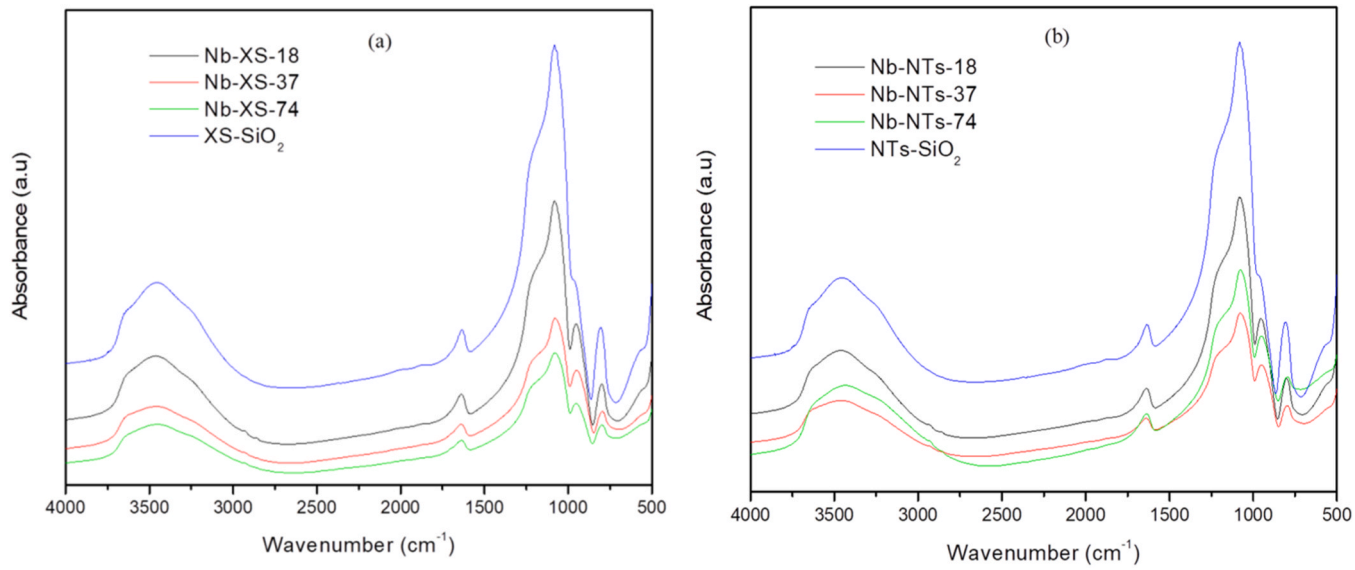

Fig. 6. ATR-FTIR spectra of (a) Nb-XS and (b) Nb-NTs catalysts after calcination at 600 °C.

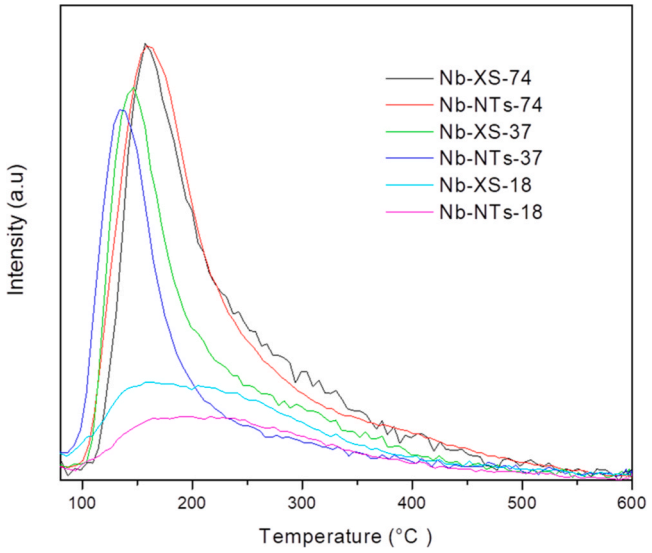

Fig. 7. NH_3-TPD profiles of the niobosilicate catalysts.

Table 3
Acid site properties of Nb-silicate catalysts.

Material	Weak acidity (mmol/g)	Medium acidity (mmol/g)	Total acidity (mmol/g)
XS-SiO_2	0.0	0.0	0.0
Nb-XS-74	0.29	0.07	0.36
Nb-XS-37	0.15	0.11	0.26
Nb-XS-18	0.10	0.02	0.12
NTs-SiO_2	0.0	0.0	0.0
Nb-NTs-74	0.25	0.07	0.33
Nb-NTs-37	0.16	0.03	0.20
Nb-NTs-18	0.0	0.08	0.08

No further increase in the solketal yield was noticed following the addition of the catalysts. These observations are in agreement with other glycerol acetalization reactions reported similar conversion at plateau, when working under similar reaction conditions [66,67]. This kinetic study showed that, at any reaction time, the XS-Nb-74 catalyst is more active than Nb-NTs-74 in terms of glycerol conversion (Fig. 8**a**) and solketal yield (Fig. 8**b**). A maximum conversion of 55 % and 45 % was recorded upon using Nb-XS-74 and Nb-NTs-74 respectively.

Based on the kinetic study, a time of 6 h was deduced to be an adequate reaction time to evaluate the catalytic activities of the solids. A catalytic screening of all Nb(V)-based catalysts has been carried under the following experimental conditions: reaction temperature of 50 °C and 10 mg of catalyst amount for 6 h of reaction. The catalytic results are reported in Table 4. The catalytic activity of our catalysts was expressed in terms of turnover number (TON) and turnover frequency (TOF) where TON (Turnover number) is expressed as moles of glycerol converted per mole of Nb atoms. TOF is the TON per unit time. The reproducibility was checked by performing the reaction three times under the optimized reaction conditions. Initially, blank experiments (XS-SiO_2 and NTs-SiO_2) carried out under the same reaction conditions (Table 4, entries 1 and 6) evidenced the absence of significant activity, thus showing that neither XS-SiO_2 nor NTs-SiO_2 exhibited catalytic sites able to promote the acetalization reaction. For all the catalysts tested at 50 °C, the selectivity to solketal was extremely high at equilibrium conversions, and no significant amount of six-membered-ring (6MR) was observed even at lower conversions. The selectivity of 5-membered ring solketal is comparatively higher than that of the 6-membered acetal, due to the axial methyl groups in the chair conformation repulsively interacting with the two hydrogen atoms in the other axial position of the 6-membered ring, leading the solketal to be thermodynamically more stable than the 6-membered acetal [68]. Nb-XS-74 and Nb-NTs-74 catalysts (Table 4, entries 2 and 7) appear to be substantially more active in the acetalization reaction, achieving up to 40 % and 30 % of solketal yield respectively, while the other catalysts markedly displayed lower catalytic performances. This is probably due to the better dispersion of Nb species on the support surface as a result of high acidic population and hydrophobic surface revealed by previous characterizations. For both series of catalysts (Nb-XS and Nb-NTs), the catalytic performance in terms of solketal yield, TON and TOF is higher in catalysts with Si/Nb ratio of 37 than those with Si/Nb ratio of 18 although no large difference was noticed upon measuring the hydrophilicity of the mentioned catalysts (compare entry 3 with 4 and entry 8 with 9 Table 4). This can be attributed to the number of acidic sites which are higher in Nb-37 catalysts (Table 3). This dominant factor, in addition to the higher surface area in catalysts having Si/Nb ratio of 37,

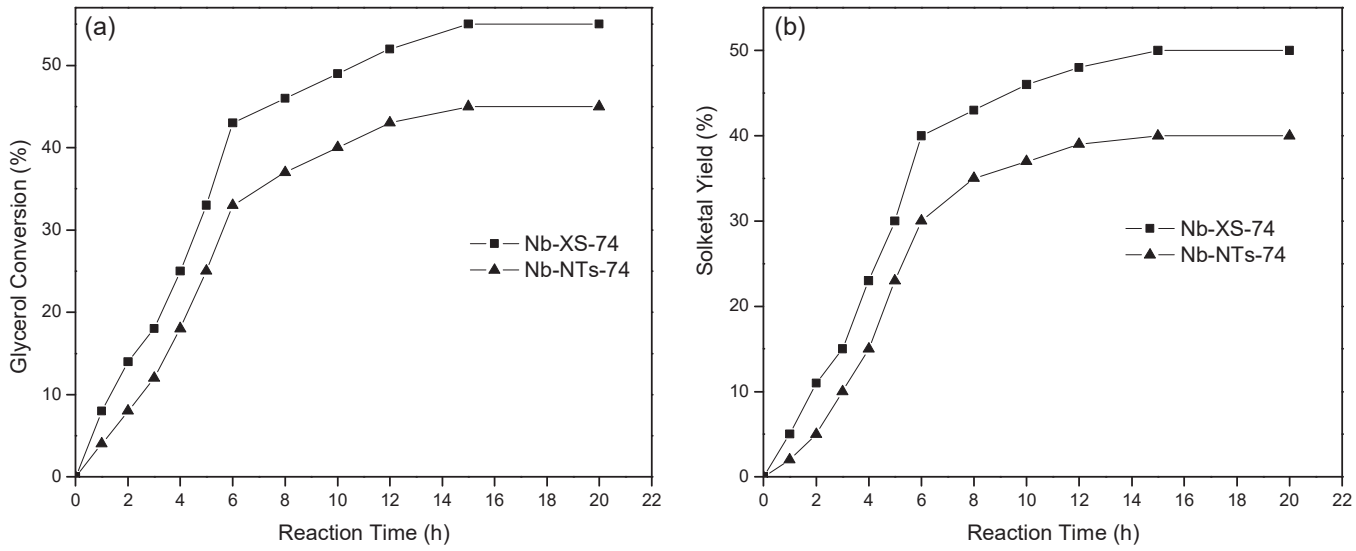

Fig. 8. Effect of reaction time using Nb-XS-74 and Nb-NTs-74 catalysts on (a) glycerol conversion, (b) solketal yield. Reaction conditions: catalyst amount 10 mg, acetone/glycerol ratio 4/1, 50 °C.

Table 4
Catalytic activity of niobosilicates materials in the conversion of glycerol to solketal.

Entry	Catalyst	Y_{SK} (%)	TON	TOF (h^{-1})	S_{SK} (%)
1	XS-SiO_2	0	0	0	0
2	Nb-XS-74	40	2054	342	95
3	Nb-XS-37	32	754	124	92
4	Nb-XS-18	23	315	52	91
5	Nb_2O_5-XS-74	0	0	0	0
6	NTs-SiO_2	0	0	0	0
7	Nb-NTs-74	30	1540	256	94
8	Nb-NTs-37	22	513	86	92
9	Nb-NTs-18	15	205	35	90
10	Nb_2O_5-NTs-74	0	0	0	0
11	Nb_2O_5	0	0	0	0

Reaction conditions: catalyst amount 10 mg, acetone/glycerol molar ratio 4/1, 50 °C, 6 h.
TON (Turnover number) is expressed as moles of glycerol converted per mole of Nb atoms. TOF is the TON per unit time.

was responsible for the higher catalytic performance of these catalysts.

When comparing catalysts of same Si/Nb ratio, Nb-XS catalysts showed higher catalytic performance in terms of Y_{SK}, TON and TOF than Nb-NTs catalysts. This can be explained by the fact that in general, pure XS-SiO_2 support is more hydrophobic than NTs-SiO_2. The clear effect of hydrophobicity in glycerol acetalization was also deduced by Stawicka group [45], where all the synthesized MCF-based catalysts exhibited a high selectivity towards solketal (97 %) due their hydrophobic nature.

For the sake of comparison, two additional solids were prepared by impregnating XS-SiO_2 and NTs-SiO_2 materials with a suspension of pre-formed Nb_2O_5 particles using a Si/Nb ratio of 74 (entries 5 and 10). Negligible catalysts activity was reported in both cases suggesting that generation of finely dispersed Nb_2O_5 species at the surface of both supports was not achieved in contrast to high and stable dispersion of niobium species obtained during impregnation of peroxo-Nb(V) precursors on different surfaces of siliceous supports. Also, extra-framework Nb was not active in our target reaction since no solketal formation was observed for Nb_2O_5 (entry 11).

The catalytic activity of all the screened catalysts in terms of TON is in direct correlation with the acidity and hydrophilicity (Fig. 9) which proves that not only the presence of acid sites is required for catalyzing the acetalization reaction, but also a sufficient hydrophobicity (less hydrophilic surface) of the catalyst surface is necessary to achieve good catalytic activity. This is in total agreement with the conclusion deduced in a review paper [69] which states, after considering various studies summarized, that both the acidic and the hydrophobic character of the catalyst surface (enhanced in some cases by niobium species) as well as the presence of mesoporosity are important for the achievement of a very high catalytic performance in the glycerol acetalization reaction.

Comparison of our synthesized niobosilicate materials to other Nb-based heterogeneous catalysts reported in the literature for the conversion of glycerol to solketal is not straightforward due to the different conditions used for the catalytic tests in different works [70]. In these studies, the catalysts are mostly prepared from niobium oxide as Nb source instead of a molecular Nb precursor from one hand, and different techniques [71] are applied during the synthesis such as microwave irradiation (Table S2). Interestingly, the conversion of glycerol using the metallosilicate NbMCF [44] achieved a glycerol conversion of 48 % and almost a total selectivity to solketal of 99 % with 2/1 acetone/glycerol molar ratio, 40 °C and 180 min which is higher than the results obtained using Nb-XS-74 and Nb-NTs-74 under same molar ratio but with higher temperature and reaction time. Such observation can be ascribed to the fact that the surface molar ratio Si/Nb of NbMCF catalyst is lower than Si/Nb ratio of our studied catalysts (Si/Nb is 91 and 95 for Nb-XS-74 and Nb-NTs-74 respectively), thus leading to better dispersion and more accessible Nb active sites for the reactants favoring a better catalytic performance.

In an attempt to compare our catalysts with other metal-based silicates (other than Nb-based catalysts), additional experiments were performed employing t-butanol as a solvent (Fig. 10). The results gathered evidence a higher catalytic performance of our Nb-based catalysts compared to some previously reported metal-containing silicates. This behavior could be due to a favorable combination of features such as high surface area, accessible mesoporosity and insertion of niobium mainly as single sites in the silica architecture.

The influence of the experimental variables such as catalysts amount, temperature and acetone/glycerol molar ratio were also studied. The influence of the catalyst amount was investigated at different temperatures 25 °C, 50 °C and 80 °C and the representative tests are reported in Fig. S5. The catalyst loading was varied from 5 to 25 mg while the other reaction parameters were kept constant. In absence of catalysts, no solketal formation was observed. The increase in the catalyst loading from 5 mg to 10 mg increases the number of active sites, causing a significant enhancement in the solketal yield. Whereas, the catalytic

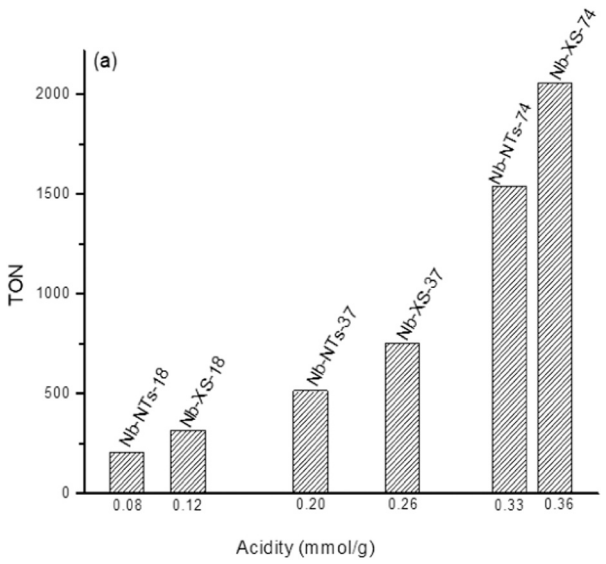

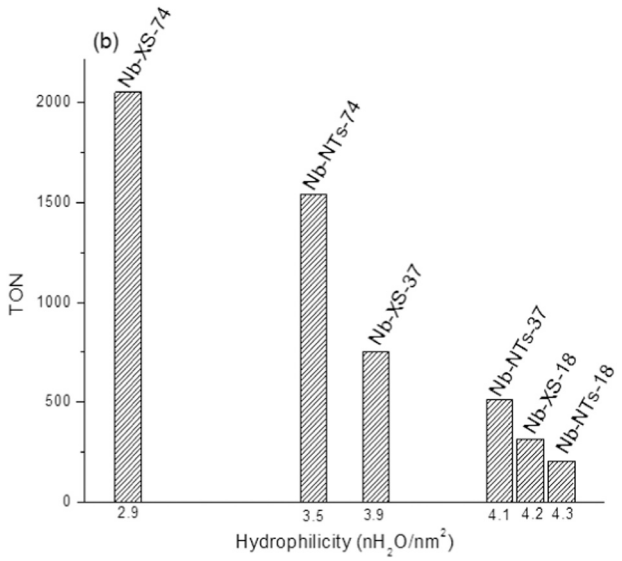

Fig. 9. Graphical correlation between TON and acidity/hydrophilicity of the studied catalysts.

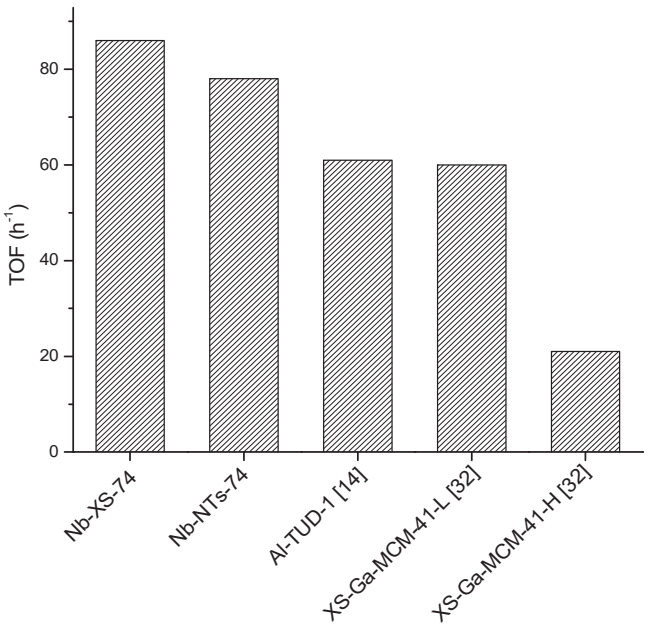

Fig. 10. Comparison of the catalytic activity of Nb-XS-74 and Nb-NTs-74 with other metal-based catalysts reported in literature. Reaction conditions: 25 mg of catalyst, 1.48 g t-butanol, 1/1 acetone/glycerol, 80 °C, 6 h.

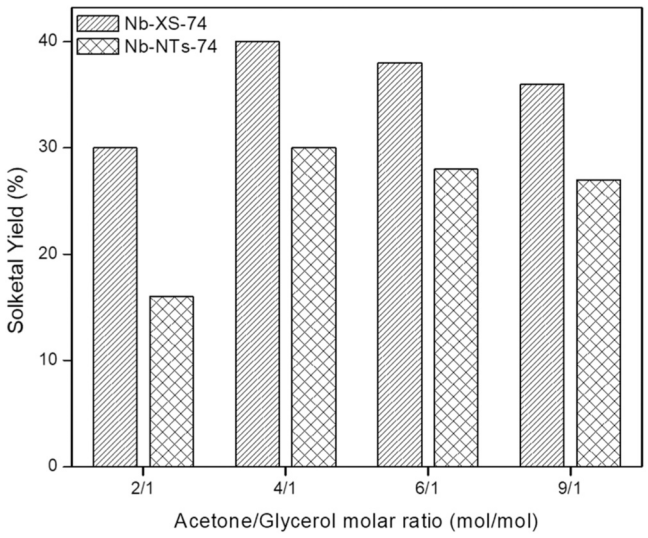

Fig. 11. Effect of acetone/glycerol molar ratio on the yield of solketal using Nb-XS-74 and Nb-NTs-74 catalysts. Reaction conditions: catalyst amount 10 mg, 50 °C, 6 h.

activity was not improved by a further increase of the catalyst loading to 25 mg. This result can be ascribed to the fact that the reaction had already reached equilibrium with 10 mg catalyst loading. This is in line with Shen et al. [15] which showed that an excess of catalyst amount is not necessarily beneficial because an equilibrium conversion is already reached with 50 mg of catalyst.

Low solketal yields were obtained at 25 °C. This decrease in the catalytic performance may be also ascribed to the intrinsic difficulties of the selected reaction conditions due to the high viscosity of glycerol which can be responsible for diffusion limitations [72]. A significant increase was obtained upon increasing the temperature to 50 °C and 80 °C.

Since glycerol acetalization with acetone is a reversible reaction, using higher molar ratio of one reactant will push the thermodynamic equilibrium towards the product and facilitate its chemisorption over the active centers of the catalysts, which is the first step of the catalytic cycle, thus justifying the rise in glycerol conversion levels. To evaluate this, the reaction was studied by varying the acetone to glycerol from 2/1–9/1 (Fig. 11). It is reported that a higher acetone to glycerol molar ratio causes a significant enhancement in the yield of solketal [25]. As expected, the increase in acetone/glycerol molar ratio up to 4/1 molar ratio causes an enhanced yield in solketal. This can be explained by the fact that the viscosity of the reaction mixture decreases and the rate of mass transfer increases with increasing amount of acetone. The further increase in the molar ratio of acetone to glycerol did not show a substantial improvement of the catalytic performances and a decrease in solketal yield was observed upon increasing the molar ratio to 9/1. The extensive quantity of acetone in the reaction mixture can cause a partial saturation of the active sites as well as an increasing of the total volume of the reaction mixture [73].

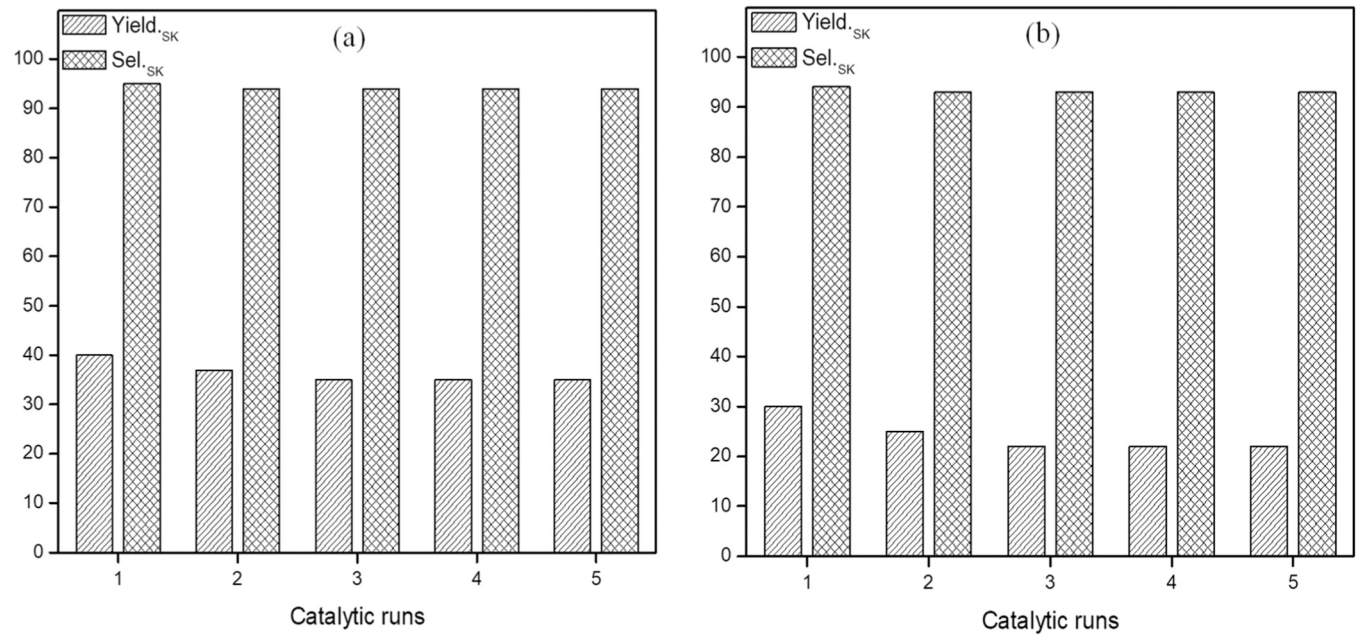

Fig. 12. Recycling test results using (a) Nb-XS-74 and (b) Nb-NTs-74 catalysts. Reaction conditions: 0.04 mol glycerol, 0.16 mol acetone, 40 mg catalyst, 6 h, 50 °C.

3.3. Catalysts reusability

In order to confirm the stability and heterogeneity of Nb-XS-74 and Nb-NTs-74 materials, recyclability tests were carried out using a thermal treatment at 500 °C (Fig. 12). In both cases, around 5 % of conversion was decreased in the first cycle probably due to the residual reactants or products being trapped within the pores or strongly adhered with the active sites of both catalysts. Nevertheless, after the first cycle, no significant change in the solketal yield was observed and the solketal selectivity was always found to be 94–95 % until the fifth cycle. This indicates that a thermal treatment at 500 °C is necessary to remove the reaction residues and fully reactivate the catalysts. Further, the spent catalysts were characterized by TEM and XRD. TEM images of the spent catalysts did not show any difference in the morphology (Fig. S6). Similarly, XRD pattern (Fig. S7) of the spent catalysts showed similar peak pattern as that of the fresh catalysts. Overall results obtained from the characterization of the spent catalysts reinforced the stable nature of the catalysts.

In order to eliminate the influence of possible leaching of active sites, hot filtration experiments were performed after 1 h at 50 °C. Fig. S8 shows that after removing catalysts from the reaction mixture, no additional conversion of glycerol was detected. This result proves that leaching of active sites is negligible. Further, inductively coupled plasma-optical emission spectrometry (ICP-OES) analysis of supernatants after the reaction did not show any detectable amounts (< 1 ppm) indicating that no niobium was lost by leaching. This observation confirms that the catalytic process is heterogeneous in nature.

4. Conclusion

Nb-incorporated mesoporous silicas (Nb-XS and Nb-NTs) were successfully synthesized by wet impregnation and applied as solid acid catalysts on the reaction of acetalization of acetone with glycerol yielding solketal. All the prepared Nb-based materials displayed acid sites that act as active sites for catalyzing the glycerol acetalization reaction. The catalytic activity of the niobosilicate materials can be explained based on the presence of accessible acid sites and required taking into account the hydrophilicity of the catalysts surface, with the more hydrophobic catalysts giving the best catalytic performance. Moreover, the Nb-XS-74 and Nb-NTs-74 catalysts are truly heterogeneous as no leaching of niobium species was detected as they retained their activity in successive catalytic cycles. The robustness of the Nb-silica materials was also supported via characterization of the solids after the 5th cycle.

CRediT authorship contribution statement

Hussein Hussein: Investigation, Validation, Data Curation, Writing - Original Draft, Visualization. **Carmela Aprile:** Conceptualization, Resources, Writing - Review & Editing, Supervision, Funding acquisition. **Michel Devillers:** Conceptualization, Resources, Writing - Review & Editing, Supervision, Funding acquisition.

Declaration of Competing Interest

The authors declare that they have no known competing financial interests or personal relationships that could have appeared to influence the work reported in this paper.

Data availability

Data will be made available on request.

Acknowledgments

The authors acknowledge the “Communauté française de Belgique” for financial support, including the PhD fellowship of H. Hussein, through the ARC programme PolarCat (15/20-069). This research used resources of the nuclear magnetic resonance service of the “Plateforme Technologique Physico-Chemical Characterization” – PC^2, located at the University of Namur.

Appendix A. Supporting information

Supplementary data associated with this article can be found in the online version at doi:10.1016/j.apcata.2023.119444.

References

[1] T.S. de Andrade, M.M.V.M. Souza, R.L. Manfro, Renew. Energy 160 (2020) 919–930.
[2] W. Hu, Y. Zhang, Y. Huang, J. Wanga, J. Gao, J. Xu, J. Energy Chem. 24 (2015) 632–636.
[3] G. Sanchez, V. Gaikwad, C. Holdsworth, B. Dlugogorski, E. Kennedy, M. Stockenhuber, J. Energy Chem. 291 (2016) 279–286.
[4] C. Xu, Y. Du, C. Li, J. Yang, G. Yang, Appl. Catal. B 164 (2015) 334–343.
[5] J. Diwakar, V. Nagabhatta, S. Kumar, A. Kumar, S.K. Saxena, Sustain. Energy Fuels 2 (2018) 1693–1698.
[6] C. Ferreira, A. Araujo, V. Calvino-Casilda, M.G. Cutrufello, E. Rombi, A.M. Fonseca, M.A. Bañares, I.C. Neves, Microporous Mesoporous Mater. 271 (2018) 243–251.
[7] M. Jose, M.G. Teixeira, D.M. Chaves, Z. Siqueira, Fuel 281 (2020), 118724.
[8] F.D.L. Menezes, M.D.O. Gumaraes, M.J. de Silva, Ind. Eng. Chem. Res. 52 (2013) 16709–16713.
[9] Z. Gui, N. Zahrtmann, S. Saravanamurugan, I. Reyero, Z. Qi, M.A. Bañares, A. Riisager, E.J. Garcia-Suarez, Chem. Sel. 1 (2016) 5869–5873.
[10] G.S. Dmitriev, A.V. Terekhov, L.N. Zanaveskin, S.N. Khadzhiev, K.L. Zanaveskin, A. L. Masksimov, Russ. J. Appl. Chem. 896 (2019) 1619–1624.
[11] P.A. Oliveira, R.O.M.A. Souza, C.J.A. Mota, J. Braz. Chem. Soc. 27 (2016) 1832–1837.
[12] X. Li, Y. Jiang, R. Zhou, Z. Hou, Appl. Clay Sci. 174 (2019) 120–126.
[13] M.R. Nanda, Y. Zhang, Z. Yuan, W. Qin, H.S. Ghaziaskar, C. Xu, Renew. Sust. Energy Rev. 56 (2016) 1022–1031.
[14] L. Li, T.I. Korányi, B.F. Sels, P.P. Pescarmona, Green. Chem. 14 (2012) 1611–1619.
[15] G. Shen, Z. Li, J.S. Park, Z. Li, G. Li, G.H. Hong, J. Lee, H. Moon, J.M. Kim, M. Jin, Mol. Catal. 520 (2022), 112179.
[16] L. Aguado-Deblas, R. Estevez, M. Russo, V. La Parola, F.M. Bautista, M.L. Testa, J. Environ. Chem. Eng. 10 (2022), 108628.
[17] Y. Jiang, R. Zhou, B. Ye, Z. Hou, J. Ind. Eng. Chem. 110 (2022) 357–366.
[18] D. Juliano, F. Mirante, S.S. Balula, Molecules 27 (19) (2022) 6573.
[19] M.J. da Silva, A.A. Julio, F.C.S. Dorigetto, RSC Adv. 5 (2015) 44499–44506.
[20] L. Chen, B. Nohair, D. Zhao, S. Kaliaguine, ChemCatChem 10 (8) (2018) 1918–1925.
[21] Y. Leng, J. Zhao, P. Jiang, D. Lu, Catal. Sci. Technol. 6 (2016) 875–881.
[22] A.X. da Silva, V.L. Gonçalves, C.J. Mota, Green. Chem. 11 (2009) 38–41.
[23] G.L. Catuzo, C.V. Santilli, L. Marti, Catal. Today 381 (2021) 215–223.
[24] M.V. Rodrigues, C. Okolie, C. Sievers, L. Martins, Cryst. Growth Des. 19 (2019) 231–241.
[25] N.J. Venkatesha, Y.S. Bhat, B.S. Jai Prakash, RSC Adv. 6 (2016) 18824–18833.
[26] J. Silvestre-Albero, M.E. Domine, J.L. Jordá, M.T. Navarro, F. Rey, F. Rodríguez-Reinoso, A. Corma, Appl. Catal. A-Gen. 507 (2015) 14–25.
[27] R. Sanchez-Vazquez, C. Pirez, J. Iglesias, K. Wilson, A.F. Lee, J.A. Melero, ChemCatChem 5 (4) (2013) 994–1001.
[28] S. An, Y. Sun, D. Song, Q. Zhang, Y. Guo, Q. Shang, J. Catal. 342 (2016) 40–54.
[29] Y. Han, D. Zhang, Curr. Opin. Chem. Eng. 1 (2) (2012) 129–139.
[30] D. Wang, X. Chen, J. Feng, M. Sun, J. Chromatogr. A 1675 (2022), 463157.
[31] J.X. Wang, L.X. Wen, Z.H. Wang, M. Wang, L. Shao, J.F. Chen, Scr. Mater. 51 (11) (2004) 1035–1039.
[32] X. Collard, L. Li, W. Lueangchaichaweng, A. Bertrand, C. Aprile, P.P. Pescarmona, Catal. Today 235 (2014) 184–192.
[33] L. Li, X. Collard, A. Bertrand, B.F. Sels, P.P. Pescarmona, C. Aprile, J. Catal. 314 (2014) 56–65.
[34] L. Soumoy, C. Celis, D.P. Debecker, M. Armandi, S. Fiorilli, C. Aprile, J. Catal. 411 (2022) 41–53.
[35] M. Ziolek, Catal. Today 78 (1–4) (2003) 47–64.
[36] N. Marin-Astorga, J.J. Martinez, D.N. Suarez, J. Cubillos, H. Rojas, C.A. Ortiz, Curr. Org. Chem. 16 (23) (2012) 2797–2801.
[37] J. Souza, P.M.T.G. Souza, P.P. de Souza, D.L. Sangiorge, V.M.D. Pasal, L.C. A. Oliveira, Catal. Today 213 (2013) 65–72.
[38] L. Zhang, J.Y. Ying, AIChE J. 43 (1997) 2793–2801.
[39] S. Vetrivel, A. Pandurangan, Catal. Lett. 99 (2005) 141–150.
[40] K. Stawicka, P. Decyk, A. Wojtaszek-Gurdak, M. Ziolek, Catal. Today 325 (2019) 2–10.
[41] H. Hussein, A. Vivian, L. Fusaro, M. Devillers, C. Aprile, ChemCatChem 12 (2020) 5966–5976.
[42] R. Rodrigues, D. Mandelli, N.S. Gonçalves, P.P. Pescarmona, W.A. Carvalho, J. Mol. Catal. A–Chem. 422 (2016) 122–130.
[43] L.C. Kao, W.C. Kan, R.M. Martin-Aranda, M.O. Guerrero-Perez, M.A. Bañares, S.Y. H. Liou, Catal. Today 356 (2020) 80–87.
[44] K. Stawicka, A.E. Diaz-Alvarez, V. Calvino-Casilda, M. Trejda, M.A. Bañares, M. Ziolek, J. Phys. Chem. C 120 (2016) 16699–16711.
[45] V. Calvino-Casilda, K. Stawicka, M. Trejda, M. Ziolek, M.A. Bañares, J. Phys. Chem. C 118 (2014) 10780–10791.
[46] D. Bayot, B. Tinant, M. Devillers, Catal. Today 78 (2003) 439–447.
[47] D. Bayot, B. Tinant, B. Mathieu, J. Declercq, M. Devillers, Eur. J. Inorg. Chem. (2003) 737–743.
[48] N. Godard, X. Collard, A. Vivian, L.A. Bivona, S. Fiorilli, L. Fusaro, C. Aprile, Appl. Catal. A–Gen. 556 (2018) 73–80.
[49] L. Huang, M. Kruk, Chem. Mater. 27 (2015) 679–689.
[50] K. Lin, P.P. Pescarmona, K. Houthoofd, D. Liang, G. Van Tendeloo, P.A. Jacobs, J. Catal. 263 (2009) 75–82.
[51] M. Catauro, C. Pagliuca, L. Lisi, G. Ruoppolo, Thermochim. Acta 381 (2002) 65–72.
[52] B. Saini, A.P. Tathod, S.K. Saxena, S. Arumugam, N. Viswanadham, ACS Sustain. Chem. Eng. 10 (2022) 1172–1181.
[53] M. Jaroniec, L.A. Solovyov, Langmuir 22 (2006) 6757–6760.
[54] M. Kruk, M. Jaroniec, A. Sayari, J. Phys. Chem. B 101 (1997) 583–589.
[55] L.A. Bivona, A. Vivian, L. Fusaro, S. Fiorilli, C. Aprile, Appl. Catal. B: Environ. 247 (2019) 182–190.
[56] G.S. Nair, E. Adrijanto, A. Alsalme, I.V. Kozhevnikov, D.J. Cooke, D.R. Brown, N. R. Shiju, Catal. Sci. Technol. 2 (2012) 1173–1179.
[57] S.M. Loverde, V. Ortiz, R.D. Kamien, M.L. Klein, D.E. Discher, Soft Matter 6 (2010) 1419–1425.
[58] Y. Geng, D.E. Discher, J. Am. Chem. Soc. 127 (2005) 12780–12781.
[59] S. Damyanova, L. Dimitrov, L. Petrov, P. Grange, Appl. Surf. Sci. 214 (2003) 68–74.
[60] P. Carniti, A. Gervasini, M. Marzo, J. Phys. Chem. C 112 (2008) 14064–14074.
[61] M. Selvaraj, S. Kawi, D.W. Park, C.S. Ha, J. Phys. Chem. C 113 (2009) 7743–7749.
[62] M. Ziółek, I. Sobczak, A. Lewandowska, I. Nowak, P. Decyk, M. Renn, B. Jankowska, Catal. Today 70 (2001) 169–181.
[63] A. Gallo, C. Tiozzo, R. Psaro, F. Carniato, M. Guidotti, J. Catal. 298 (2013) 77–83.
[64] C. Tiozzo, C. Bisio, F. Carniato, L. Marchese, A. Gallo, N. Ravasio, R. Psaro, M. Guidotti, Eur. J. Lipid Sci. Technol. 115 (2013) 86–93.
[65] J.M.R. Gallo, H.O. Pastore, U. Schudardt, J. Non-Cryst. Solids 354 (2008) 1648–1653.
[66] M.N. Moreira, R.P.V. Faria, A.M. Ribeiro, A.E. Rodrigues, Ind. Eng., Chem. Res. 58 (2019) 17746–17759.
[67] F. Taddeo, R. Esposito, V. Russo, M. Di Serio, Catalysts 11 (2021) 83.
[68] L.P. Ozorio, R. Pianzolli, M. Beatriz, S. Mota, C.J.A. Mota, J. Braz. Chem. Soc. 23 (5) (2012) 931–937.
[69] L. Oliveira, M. Pereira, A. Pacheli Heitman, J. Filho, C. Oliveira, M. Ziolek, Molecules 28 (2023) 1527.
[70] T.E. Souza, I.D. Padula, M.M.G. Teodoro, P. Chagas, J.M. Resende, P.P. Souza, L.C. A. Oliveira, Catal. Today 254 (2015) 83–89.
[71] A. Feliczak-Guzik, I. Nowak, Microporous Mesoporous Mater. 277 (2019) 301–308.
[72] G. Arun, M. Ayoub, Z. Zulqarnain, U. Deshannavar, M.H.M. Yusoff, S. Farrukh, F. Sher, Catalysts 11 (2021), 1537.
[73] M.J. da Silva, A.A. Rodrigues, P.F. Pinheiro, Fuel 267 (2020), 118164.